ELSEVIER

Physica A 242 (1997) 119–140

PHYSICA A

Heat transfer in pure critical fluids surrounded by finitely conducting boundaries in microgravity

R. de Bruijn[a,*], R.J.J. van Diest[a], T.D. Karapantsios[a], A.C. Michels[a], W.A. Wakeham[b], J.P.M. Trusler[b]

[a] *Van der Waals-Zeeman Institute, University of Amsterdam, Valckenierstraat 65 1018 XE Amsterdam, Netherlands*

[b] *Department of Chemical Engineering, Imperial College, Prince Consort Road, London SW7 2BY, UK*

Received 22 August 1996

Abstract

The behaviour of a near-critical sample of SF_6, bounded by container walls with finite thermal properties, was studied in space during the 1994 IML-2 mission. Experiments were performed in the range 2500 to 1 mK above the critical point in which simultaneous density and temperature measurements are conducted during a number of transient heating runs. The results of these measurements show clearly that a fast isentropic thermalization takes place uniformly throughout the sample, with essentially no effect on existing temperature and density gradients. The temperature rise caused by the isentropic thermalization is described quantitatively by a theoretical expression which takes into account the finite thermal impedance of the cell walls. It has been possible to do so in a manner that satisfactorily represents the observations. The success of this description enables the separation of isentropic thermalization from true heat transport effects, thereby opening the way to a determination of the thermal diffusivity of the fluid at temperatures as close as 1 mK to the critical temperature. In addition, the observed isentropic compressive heating mechanism suggests a new way for assessing specific important thermodynamic properties in the critical region, based on the experimental determination of the isentropic thermal expansion coefficient.

PACS: 44.10.+i; 64.60.Fr; 66.10.Cb; 5.70.Jk
Keywords: Critical region; Heat transport; Adiabatic effect

1. Introduction

In the neighbourhood of the critical point (CP) of a pure fluid, many of its thermodynamic and transport properties display singular behaviour. Some, such as the

* Corresponding author.

PII S0378-4371(97)00197-0

compressibility and thermal conductivity, on approaching CP tend to infinity, while others, such as the thermal diffusivity, go to zero [1].

Quantitative experimental corroboration of the theories that have been developed to account for this behaviour is, especially close to CP, incomplete (cf. [2]). On earth, owing to the combined effect of a gravitational field and the compressibility of the fluid, one can realize the critical state only in a narrow horizontal layer of a fluid sample. Additionally, the introduction of a temperature gradient in a fluid to study heat transport inevitably leads to spurious convective contributions to this process. For these reasons it has not been possible to probe reliably either the thermal conductivity λ or the thermal diffusivity D_T of a sample at the critical density much closer to CP than about 100 mK [3]. Thus experimental verification of the true singular behaviour has been indirect and has relied upon extensions of the theory into a region farther from CP, where it is necessarily less exact, but where comparisons with experiment have been possible. The ultimate aim of the work upon which we are engaged and of which the present paper represents a part is the determination of λ and D_T of a pure fluid in the near-critical region.

In order to determine λ or D_T to within say 1 mK from CP, a microgravity environment is of special value because it provides a means to eliminate density stratification and convection. From the early stages of this work it was realized however [4–7] that under these conditions another process of temperature change in a fluid (referred to as *the adiabatic effect* (AE) or *piston effect*) becomes of increasing significance during any transient heating as CP is approached. Fundamentally, this AE is not a mechanism of true heat transport (contrary to the statements made in some of the literature); rather, it is a temperature change resulting from isentropic compression in a finite sample. Heating at the boundary of such a sample causes thermal expansion of the adjacent fluid layer and, consequently, a pressure increase everywhere in the fluid. This pressure increase results in an essentially adiabatic increase in temperature and density throughout the fluid. Various experiments confirming the uniform rapid thermal response in a near-critical fluid have been reported by Boukari et al. [8], who used ground-based equipment, and by Bonetti et al. [9], Straub et al. [10] and Michels et al. [11] working on microgravity platforms.

The interpretation of the AE in a practical system is complicated by the fact that it introduces an additional heat flow through the walls surrounding the fluid. During the rapid uniform temperature increase these walls remain colder than the fluid itself and a boundary layer develops at these walls: energy will flow out of the fluid, cooling it again by adiabatic expansion. Ferrell and Hao [12] studied analytically the AE including this secondary effect, following a model in which the fluid is initially at a uniform temperature that is different from that of the container. They concluded that this secondary effect depends on the ratio between thermal properties of the wall material and those of the fluid; since the latter exhibit singular behaviour near CP, the fraction of heating power dissipated through thermal conduction, in terms of distance to CP, will depend strongly on actual thermal parameters of the walls. Beysens et al. [13] experimentally confirmed this effect qualitatively. However,

to account for it in a quantitative way one has to calculate the overall cell wall parameters which, for most actual cell configurations cannot be accomplished with reasonable accuracy.

Such a quantitative description of the AE is necessary if measurements of the transient temperature increase in a fluid near the critical point are to be used to study λ and D_T in the near-critical region. This is because the AE-contribution must be eliminated from the measurements of temperature rise before they are interpreted in terms of a simple conduction equation.

The work reported here concerns a quantitative description of the AE in measurements in a sample of near-critical SF_6 under microgravity conditions, following a heating with constant power at a flat boundary surface [14] in a range down to $T - T_c = 1$ mK. This description should enable a separation of the AE from true heat transport effects in data of measurements on λ and D_T in the near-critical region of pure fluids. SF_6 was chosen as the test fluid mainly because of its convenient critical parameters ($T_c = 318.7$ K, $P_c = 3.75$ MPa and $\rho_c = 744$ kg/m^3 [15]). The measurements were performed using a custom-made test cell mounted in the European Space Agency's Critical Point Facility (CPF) [16], which was flown in the cargo bay of the Space Shuttle Columbia during the spacelab IML-2 mission, in July 1994. Density changes were observed interferometrically, while temperature changes were measured using thermistors located in and around the test cell. The total duration of the experiment was 56 h and the maximum acceleration throughout was below $10^{-4}g$. To the best of our knowledge, this is the first work in which simultaneous temperature and density measurements have been made and in which a wide range of states and heating profiles have been investigated.

A preliminary inspection of our microgravity data has been reported in a previous paper [11] where the overall capability of the system to register isentropic temperature and density changes in the fluid has been communicated. Here, we fully explore the isentropic heat transfer mechanism by conducting a thorough analysis of the performance of the experimental system, including the energy losses to the surroundings. In Section 2 a review of the theory is given where we show that the AE enables the measurement of the isentropic thermal expansion coefficient α_s as previously presented by Michels et al. [11]. Also we extend the theoretical model proposed by Ferrell and Hao [12], which presumes a stepwise temperature change, to transient heating at the boundary. The experimental configuration and procedure are presented in Section 3. The way in which temperature and density data are obtained and analyzed is communicated in Section 4, where it is also explained how we dealt with the complex geometry of our fluid container. The analysis of the results in Section 5 shows consistently the role of the AE in a pure critical fluid surrounded by finitely conducting boundaries. Our conclusions are summarized in Section 6.

2. Theory of heat transfer

We consider the transient heating of a compressible fluid of thermal conductivity λ, thermal diffusivity D_T and density ρ confined in a fixed volume V by a series of solid surfaces S_i, which themselves possess a thermal conductivity λ_i and a thermal diffusivity D_i. The transient heating of the fluid is accomplished by the application of a constant heat flow q_f at a surface S entirely contained within the fluid which is initiated at time $t=0$ and terminated at a time $t=t_p$. It is intended to study the evolution of the temperature and density in the fluid over a period of time following initiation of the heat pulse.

2.1. Temperature and density field

In order to find an expression for the temperature field in a locally heated fluid, one might investigate the problem theoretically by seeking solutions of the fully-non-linear Navier–Stokes equations, subject to appropriate boundary conditions but in the absence of a gravitational field. This is a very complicated task and two somewhat simpler approaches have been adopted in literature, both of which recognize the existence of a (short) acoustic time scale and a (longer) conduction time scale. In the first simpler approach [7], the unsteady linearized Navier–Stokes equations are solved separately in both regimes. In the second approach [4,6], a simplified one-dimensional conservation equation, the energy equation, is derived, which takes into account both thermal conduction and compression-work terms but ignores fluid flow. In these pioneering works, the thermal conductivity of the fluid container was irrelevant.

The existence of these two time scales is most readily understood by considering the effect on the pressure. On the (short) acoustic time scale, local fluctuations, caused by heating, propagate through the fluid as pressure waves; the pressure is neither constant in time nor spatially uniform. On the (longer) conduction time scale, the pressure in the system is essentially spatially uniform though not necessarily constant in time.

In the work reported here, we have adopted the second approach as this combines satisfactory accuracy with less computational effort. The equation describing the thermal field in a non-viscous compressible fluid is [17]

$$\frac{dT}{dt} - \left(1 - \frac{1}{\gamma}\right)\left(\frac{\partial T}{\partial P}\right)_\rho \frac{dP}{dt} = \frac{1}{\rho C_P}\nabla \cdot (\lambda \nabla T), \tag{1}$$

where γ is the specific heat ratio ($=C_p/C_V$) and C_p and C_V are the specific heats at constant pressure and constant volume respectively. The second term on the LHS of Eq. (1) modifies the usual thermal diffusion equation to account for the isentropic temperature and density changes accompanying variations in the pressure, i.e. the AE. Eq. (1) shows that, for a spatially uniform pressure change, this term acts uniformly across the entire fluid thereby leaving any existing temperature gradients unaltered. The term on the RHS of Eq. (1) (the conduction term) contributes only in the region where temperature gradients are present. Near to the critical point, the different characteristics

of the two terms have significant consequences which need to be understood before one attempts to make measurements of the thermal diffusivity.

Physically, the fact that $\lambda \to \infty$ in the approach to the critical point means that the heat flux provided by the heater q_f is transmitted directly to the fluid at the interface according to the boundary condition

$$\frac{q_f}{S} = -\lambda \nabla T \text{ at } S, \quad 0 \leqslant t \leqslant t_p . \tag{2}$$

However, the vanishingly small thermal diffusivity of the fluid renders the term on the right-hand side of Eq. (1) small, so that the heat is contained in a very thin layer of fluid close to the heater. However, the rapid heating and expansion of the boundary layer generates a uniform compression of the bulk of the fluid which causes an isentropic temperature increase throughout the fluid.

In order to find an expression for the changes in the density field we first write

$$\frac{d\rho}{dt} = \left(\frac{\partial \rho}{\partial T}\right)_P \frac{dT}{dt} + \left(\frac{\partial \rho}{\partial P}\right)_T \frac{dP}{dt} . \tag{3}$$

If we substitute (dP/dt) from Eq. (1) into Eq. (3), we obtain after some algebra the expression

$$\frac{d\rho}{dt} = -\frac{1}{\gamma - 1}\left(\frac{\partial \rho}{\partial T}\right)_P \left\{\frac{dT}{dt} - \frac{1}{\rho C_v}\nabla \cdot (\lambda \nabla T)\right\} . \tag{4}$$

Disregarding the spatial dependence of the pressure and neglecting the implicit spatial and time variations of the various thermodynamic coefficients, Eq. (4) leads to

$$\frac{d\rho}{dt} = -\rho \alpha_S \frac{dT}{dt} + \frac{\lambda}{C_P - C_v}\nabla \cdot \left(\frac{\nabla \rho}{\rho}\right), \tag{5}$$

where α_s is the isentropic thermal expansion coefficient. Eq. (5) readily demonstrates that the AE alters the density essentially proportional to the temperature, regardless of the distance to the critical point or of the way heat is applied to the fluid. For the region outside the developing boundary layer, i.e. in the bulk, the second term on the RHS of Eq. (5) is generally negligible. Note that, as the critical point is approached, due to the fast divergence of C_p, this term is of decreasing importance. Therefore, provided that the possible existing density gradients are small enough, simultaneous measurements of temperature and density in the bulk can provide the isentropic thermal expansion coefficient α_s.

2.2. Isentropic temperature rise

We are interested here in describing the first phase of the fluid heating during which the isentropic temperature rise takes place. Numerical solutions of Eqs. (1) and (2) show that, with heating pulses typical to this experiment, the resulting temperature and density changes are sufficiently small for the various thermodynamic coefficients of the fluid to be considered constant [11].

In the approximation that the various thermodynamic coefficients do not vary during heating, one finds, based entirely on thermodynamic considerations, that for a heat flux q_f the temperature rise outside of the boundary layer in the bulk fluid is

$$\frac{dT}{dt} = \frac{(q_f - q_\ell)}{\rho_c V C_V}\left(1 - \frac{1}{\gamma}\right). \tag{6}$$

In Eq. (6) q_ℓ represents the heat losses to the cell walls in a real experiment. These losses from the sample must be taken into account, since in a real system isentropic cooling begins simultaneously with the isentropic temperature rise [11].

Ferrell and Hao [12] studied analytically such a combined heating–cooling process, accounting for the available (for heat exchange) surface area of the container walls and the transport properties of both the fluid and the walls. Avoiding the long-term behaviour of the fluid, whenever the developing boundary layer reaches the size of the characteristic length of the cell, we reproduce from their work the solution of Eq. (6). For an amount of energy Q delivered to the fluid, all at one instant ($t = 0$), the bulk temperature variation with time is given by

$$T_b(t) = (1 - \gamma^{-1})\frac{Q}{\rho_c V C_V} e^{t^*}\, erfc\sqrt{t^*}\,, \tag{7a}$$

where $erfc = 1 - erf$ is the complimentary error function and $t^* = t/t_c$. The characteristic time t_c for the isentropic equilibration is

$$t_c = \ell_{eff}^2 / D_T\,, \tag{7b}$$

where

$$\ell_{eff}^{-1} = \frac{\gamma - 1}{V}\sum_{i=1}^{N}\frac{\sigma_i S_i}{1 + \sigma_i} \tag{7c}$$

is $(\gamma - 1)$ times a weighted sum over the inverse lengths S_i/V of the N different boundary segments. The *inverse thermal impedance ratio* σ_i is defined as

$$\sigma_i = \frac{\lambda_i}{\sqrt{D_i}} \Big/ \frac{\lambda}{\sqrt{D_T}}\,, \tag{7d}$$

and S_i is the surface area of the ith segment.

Ferrell and Hao [12] analyzed Eq. (7) and concluded that, as the critical point is approached ($T \to T_c$) and the fluid thermal impedance drops below that of the walls, a crossover takes place from a rapid decrease in characteristic time t_c, relatively far away from T_c, to a weak increase in t_c, as the square of the constant volume specific heat.

Complementing the work of Ferrell and Hao [12], for the case that energy is applied to the fluid, not instantaneously but over a finite period of time ($0 \to t_p$), Eq. (7a) is modified to

$$T_b(t) = \frac{1 - \gamma^{-1}}{\rho_c V C_V}\int_0^t q(t') e^{t'^*}\, erfc\sqrt{t'^*}\, dt'\,, \tag{8}$$

where $q(t)$ represents the time-dependent energy flux to the fluid. If further, heating pulses of constant power (q_f) are utilized to stimulate the fluid then $q(t)=q_f$ and Eq. (8) becomes accordingly

$$T_b(t)=q_f\frac{1-\gamma^{-1}}{\rho_c V C_V}\int_0^t e^{t'^*}\,erfc\sqrt{t'^*}\,dt' \tag{9}$$

which after some algebra leads to

$$T_b(t)=q_f A\left[\frac{2}{\sqrt{\pi}}\sqrt{t^*}-1+e^{t^*}erfc\sqrt{t^*}\right], \tag{10}$$

where $A=t_c(1-\gamma^{-1})/(\rho V C_V)$. This A represents an apparent amplitude in the expression above. Obviously, A strongly depends on the distance to the critical point.

Eq. (10) reveals two limiting cases both valid for $t \gg t_c$. For $\sigma_i \gg 1$, or $\tau=(T-T_c)/T_c$ is relatively large, Eq. (10) reduces to

$$T_b(t)=q_f\frac{\sqrt{D_T}}{\lambda}\left(\sum_{i=1}^{N}S_i\right)^{-1}\left[\frac{2}{\sqrt{\pi}}t^{1/2}-\sqrt{t_c}\right] \tag{11}$$

which indicates that far away from T_c the boundaries of the system can be approximately considered as infinitely conducting and their surface area is the most important parameter for the determination of the heat-loss. The temperature increase is then dictated mainly by the ratio $\sqrt{D_T}/\lambda$.

For $\sigma_i \ll 1$, or τ is relatively small, Eq. (10) yields, respectively,

$$T_b(t)=q_f\left(\sum_{i=1}^{N}\frac{\lambda_i S_i}{\sqrt{D_i}}\right)^{-1}\left[\frac{2}{\sqrt{\pi}}t^{1/2}-\sqrt{t_c}\right]. \tag{12}$$

As can be easily seen, for this particular limiting case it is the transport properties of the boundaries that govern the thermal behavior of the system. At first sight this may seem to be somewhat surprising since one would rather expect the temperature rise in the bulk $T_b(t)$ to vanish as the isochoric specific heat diverges. Interestingly, in either of these cases, Eqs. (11) and (12), a simple relation is obtained which predicts an isentropic temperature change proportional to the square root of the heating time.

3. Experimental setup and procedure

3.1. Facilities and test cell

In CPF the sample fluid is contained in a test cell, which is placed inside a thermostat. The thermostat provides extremely precise temperature stability of the order of 30 μK/h with spatial gradients of less than 10 μK/cm. The CPF is equipped with

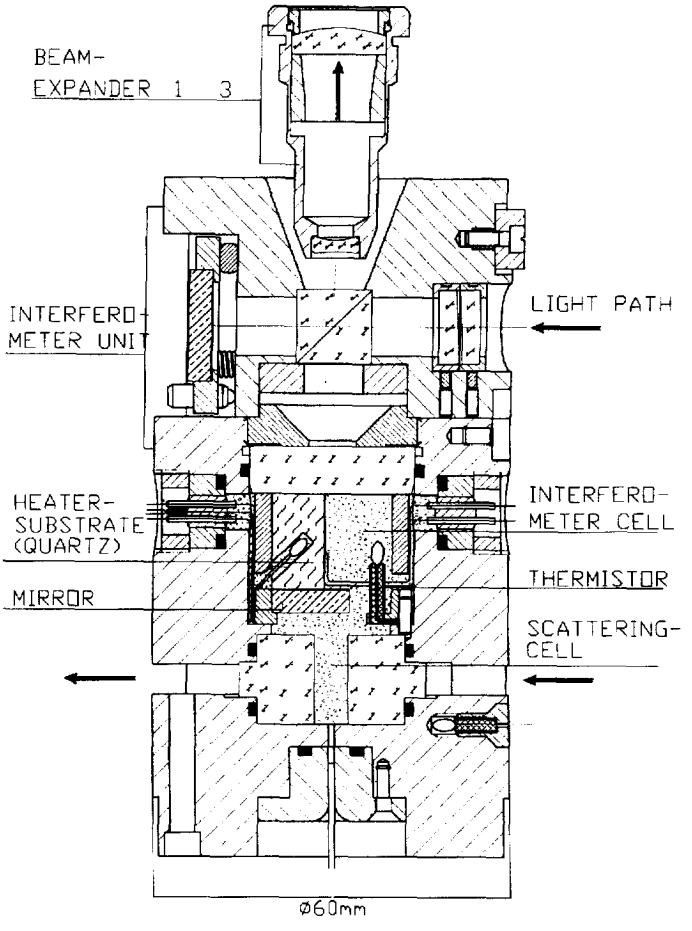

Fig. 1. The test cell.

a variety of optical and electronic systems which enable the stimulation and observation of the sample fluid. For optical measurements the CPF provides two sources of illumination: a 1 mW laser operating at 633 nm; and a light-emitting diode. Images from a Twyman–Green interferometer (IF) system and direct visualization (VIS) of the sample are observed with a video camera and a photocamera. Light scattering (LS) signals are collected on fiber-optic guides and transmitted to a photomultiplier tube. A current source system (CSS) provides a constant current up to 1 A with a resolution of 20 μA.

Our test cell, shown in Fig. 1, consists of two interconnected cylindrical chambers with a total volume of approximately 6 cm^3. The cell is filled with SF_6 at its critical density as determined by the disappearance and reappearance of the vapour–liquid meniscus in the middle of the cell. The larger chamber accommodates a mirror which forms a part of the IF system, while the smaller chamber enables LS measurements at discrete angles between 22° and 90° as well as direct visualization.

The IF chamber of the test cell is fitted with a flat quartz plate, offset by 1 mm from the optical axis (to which it is parallel). A gold layer measuring 14 mm × 15 mm and 20 nm thick is deposited on this plate and serves as the heater ($R = 3.6\ \Omega$) when a constant current passes through it utilizing the CSS. Density changes in the adjacent fluid are monitored throughout the experiment using the IF images; the field of view is 4 mm in diameter. Five high sensitivity (μK) temperature sensors (thermistors) are available for temperature measurements. One of them is located in the fluid approximately 9 mm from the heater whereas a second one is embedded in the quartz substrate behind the gold heater. The remaining thermistors are located in the wall of the cell. Unfortunately, due to an extreme offset of the thermistor in the quartz, this particular one could not be used at its highest sensitivity. (For the impact of this see Section 4.2).

The CPF is a fully automatic facility able to run an experiment on a prefixed timeline; however, its telecommanding capability proved to be absolutely essential for optimizing the operation of the experiment and frequent changes in the timeline were made during the course of the experiment.

3.2. *Experimental scenario*

The actual sequence of experimental temperatures was as follows. The sample was first heated to $T - T_c \approx 2500$ mK (48°C) and appreciable (>2 h) allowed for it to become homogeneous. It was then cooled down in steps to 1000, 300, 100, 50 and finally 15 mK above T_c. At $T_c + 15$ mK, a slow cooling ramp was initialized ending a few mK below T_c when phase separation was confirmed. The sample was again homogenized at $T - T_c \approx 2500$ mK and cooled down, in steps, to 2000, 1500 and 800 mK above T_c and then, in ramps, to 450, 150, 50, 30, 10, 5, 2 and 1 mK above T_c. Finally, the sample was heated slowly to $T_c + 100$ mK to check for hysteresis effects.

Following each change in temperature, various waiting periods were employed in an attempt to improve approximate thermodynamic equilibrium. The evidence from the IF images was that equilibrium was never reached but that with specific precautions a steady state could be achieved within reasonable time, e.g. at $T - T_c = 1$ mK in 3 h and after approaching with a slow ramp (2 mK/h).

4. Data analysis

4.1. *Temperature and density*

The readings of the various thermistors were acquired by CPF each second. The temperature indication was in the form of a difference from the set temperature of the thermostat, i.e. the temperature at which the transient heating runs were performed, which, in its turn, is defined in terms of difference to T_c. Since, moreover, it was possible to "null" all thermistors at any time, their readings could be obtained at a maximum resolution.

The capability of the fluid thermistor to trace accurately the fast, isentropic temperature changes in the bulk, as we approach the critical point, is a matter of serious concern. To investigate this issue, simple calculations of the thermistor response have been made (see the appendix a) from which a conclusion arises that the thermistor response gets better and better as T_c is approached! The physical reason for the good response near to T_c is that the heat flow through the boundary layer around the thermistor gets larger as the thermal conductivity of the fluid increases.

The IF setup permitted variations in the density to be monitored through the corresponding variations in the refractive index using the equation

$$\Delta K(x, y) = \Delta n(x, y) \frac{l(x, y)}{\Lambda}, \tag{13}$$

where ΔK is the shift in interference order, Δn is the shift in the refractive index, Λ is the laser light wavelength and $l(x, y)$ is the pathlength of light in the sample. This equation relates the interference order distribution $K(x, y)$ to the refractive index $n(x, y)$, which is further related to the density distribution $\rho(x, y)$ via the Lorentz–Lorenz expression

$$\frac{n^2 - 1}{n^2 + 2} = Q\rho\,. \tag{14}$$

For SF_6, $Q = 8.35 \times 10^{-5}\ \mathrm{m^3/kg}$ [18]. Interferograms could thus be converted to density profiles which formed the basis for further analysis.

In our setup, the sensitivity of the density measurements was $\Delta\rho/\rho \approx 10^{-5}$, which did not permit the accurate determination of the small bulk density changes associated with the gold layer heating pulses. Nevertheless, larger density changes of the bulk accompanying set temperature changes could easily be measured.

During the heating runs, video images were recorded at various times and digitized for analysis. The digitized images were analyzed along pixel rows parallel to the heater. The details of this analysis will be published later [19].

4.2. Heating pulses

When, at a set temperature, a steady state was obtained, constant-current heating pulses were applied to the fluid by the plate heater. Pulse duration was varied between 1 and 5 min. Also, using the thermistor in the fluid as the heat source, a few pulses of elevated power (5.65 mW) but with a duration of $\leqslant 5$ s were employed.

The power delivered to the system by the plate heater varied between 0.04 and 0.18 mW according to the current selected. Contrary to heating with the thermistor, this power does not go entirely to the fluid but part of it (q_s) is absorbed by the quartz substrate. This energy decomposition is dictated by the thermodynamic and transport properties of the fluid and the quartz. Knowledge of the precise amount of energy that enters the fluid is of paramount importance for the solution of Eq. (10). An obvious

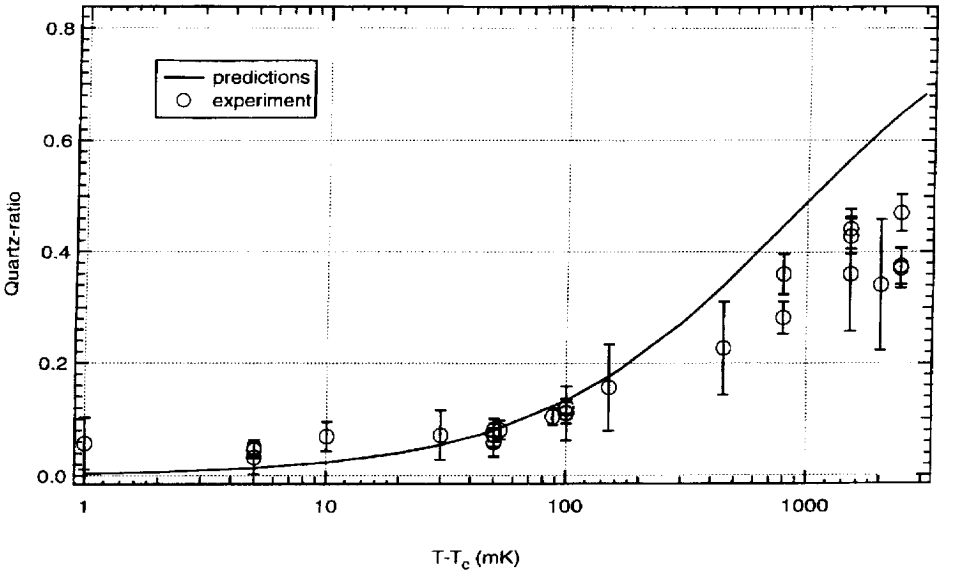

Fig. 2. Fraction of total delivered energy that enters the heater substrate.

relation for the power q_f that goes into the fluid is

$$q_f = \frac{I^2 R}{1 + q_s/q_f} \,. \tag{15}$$

In order to calculate the dissipation ratio q_s/q_f, here it is assumed that heat travels inside both the quartz and the fluid according to the well-known Fourier equation with a constant power source at the interface. In this case, the dissipation ratio is equal to the inverse impedance ratio of the fluid and the heater substrate. Note that the temperature rise due to the AE is included in the heat-loss term, i.e. the characteristic time t_c [Eq. (7b)], as the heater surface also is regarded as a heat-loss wall, thereby leaving q_f time-independent. The detailed calculations will be given elsewhere [19].

Fig. 2 shows a plot of the fraction of the total energy that enters the quartz, q_s/I^2R, at different distances to T_c. The solid line represents the predictions arising from the calculated dissipation ratio where fluid properties are taken from the equation of state (EOS) by Abbaci and Sengers [15] and diffusivity values are used from the measurements by Jany and Straub [3]; the data points come from measurements by the thermistor embedded in the quartz plate. It shows that less and less energy goes to the substrate as T_c is approached, thanks to the increasing conductivity of the fluid.

The discrepancy between measurements and predictions may be attributed to several possible sources of error. Measuring in this way, one does expect to find for high dissipations to the substrate, a q_s lower than predicted, due to inevitable losses.

Table 1
Inverse thermal impedance and surface area of wall materials

Wall materials	$\lambda_i/\sqrt{D_i}$ ($Ws^{1/2}/m^2 K$)	Si (mm^2)
Aluminum	2.4×10^4	240
Synthetic quartz	6×10^2	540
Fused silicon	6×10^2	690
KEL-F	5×10^2	470
Invar (NILO-36)	8×10^3	100
Apparent properties	6×10^3	2.5×10^3

Furthermore, when most of the dissipated energy goes to the fluid it is probable that one measures a q_s too high, due to the temperature increase of the fluid around the substrate or the thermistor wires. Taking also into account the reduced sensitivity of the thermistor in the substrate, the comparison is considered satisfactory and, henceforth, the literature values [3,15] have been used to calculate the temperature-dependent fluid-quartz impedance ratio. This ratio further is used in Eq. (15) for solving the heat transport equations on the fluid's side.

4.3. *Apparent wall properties*

In order to implement Eqs. (10)–(12) for comparisons with the data of the isentropic temperature rise in the bulk, the transport properties and the surface area of all the cell walls need to be determined. This is not an easy task because of the complex geometry of the cell and the several different materials utilized in its construction. Among the various materials of construction we have identified the five most significant in view of their relative contribution to heat losses. These five materials exhibit the highest inverse thermal impedance values together with appreciable surface areas for heat exchange. Table 1 lists these parts and their corresponding inverse impedance and surface area values. The inverse thermal impedance values are provided by the manufacturers while the surface areas are evaluated by simple geometrical considerations. However, calculating the surface areas – available for heat exchange – in a configuration of such complexity is expected to give only very conservative values since the possibility cannot be excluded that minor geometrical imperfections can have a large effect. Indeed, preliminary calculations taking into account the individual wall materials gave an unsatisfactory correlation between predicted and measured isentropic temperature changes. Therefore, as customarily adopted in the literature, it seems appropriate to include all effects in just one single set of phenomenological parameters which will be referred henceforth as the apparent inverse thermal impedance, $\lambda_a/\sqrt{D_a}$ and the apparent surface area, S_a, of the container walls. Values for these parameters may be obtained from a "best fit" procedure of Eq. (10) to experimental data. The values produced in this way are also included in Table 1. As shown, the fitted apparent inverse thermal impedance is, as expected, in the order of magnitude of the

highest impedances but the apparent surface area indeed turns out to be larger than calculated.

5. Results and discussion

The apparent critical temperature, on the scale indicated by the measurement thermistor, was determined at the time of filling (several months before the mission). During the experiment, the critical temperature was redetermined by analysis of the LS signals during the slow cooling of the test cell through T_c and by observation of the phase separation in the VIS channel. It was found that the critical temperature of the sample determined in this way was 25 mK below that determined on earth. By checking the filling of the cell we found that there is no measurable leakage and we conclude that the difference is a consequence of thermistor drift.

Altogether 66 heating runs were performed. During and following a heating run, two mechanisms of temperature change were certainly apparent. From the IF profiles we clearly see a diffusive thermal boundary layer (bent fringes) and from detailed analysis we determine a rapid spatially-uniform fringe shift which corresponds to a homogeneous density change in the bulk of the fluid (Fig. 3). The latter information is obtained by utilizing Eqs. (13) and (14) to deduce density profiles across the parts of the frames representing the bulk (far away from the developing boundary layer). It is notable that density variations in the bulk can not be observed by "the naked eye" because changes are much less than 1% of the original fringe pattern. Moreover, we have confirmed by our analysis the result of Guenoun et al. [20] that the AE does not alter any existing density gradients in the sample but acts uniformly across the fluid.

By the AE, a powerful tool is delivered to determine the isentropic thermal expansion coefficient α_s as a function of the distance to T_c in a novel, intrinsically accurate way. Recalling arguments advanced with regard to Eq. (5), simultaneous temperature and density measurements in the bulk are utilized to produce, in a direct manner, this particular isentropic coefficient. This method is especially in the critical region of definite advantage since it is independent of the energy transfer outside the bulk of the fluid. However, the particular technique used in this experiment to measure the density change is an integral average along the path of the light. One should realize that this path meets two cell-boundaries, i.e. the window and the mirror, where a boundary layer will develop during heating, in which the second term on the RHS of Eq. (5) is not negligible. When the temperature of the fluid changes, the temperature of these boundaries will stay behind that of the fluid (colder when heating and hotter when cooling) and the change in density in the developing boundary-layers will be even larger than the, isentropic, change of the bulk. The average density change along the path of the light therefore will be larger than the bulk density change. The implications of this to the measurement of α_s is beyond the scope of this paper and will be addressed in a forthcoming paper.

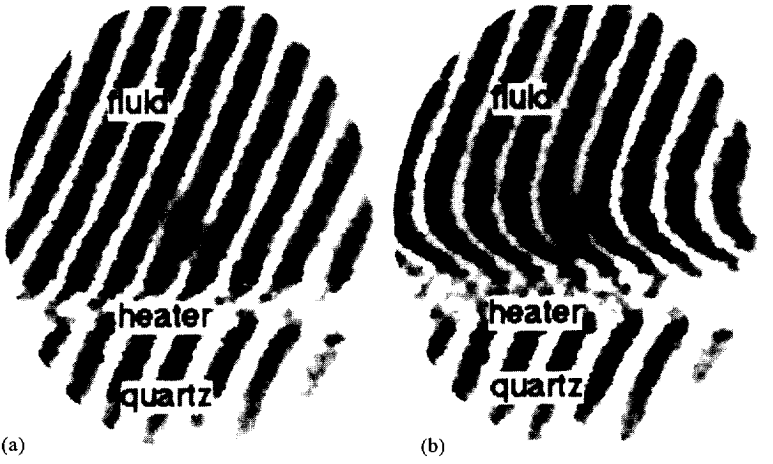

Fig. 3. Interferometry fringes (a) before heating ($t = 0$ s), and (b) at time $t = 57$ s after the onset of heating.

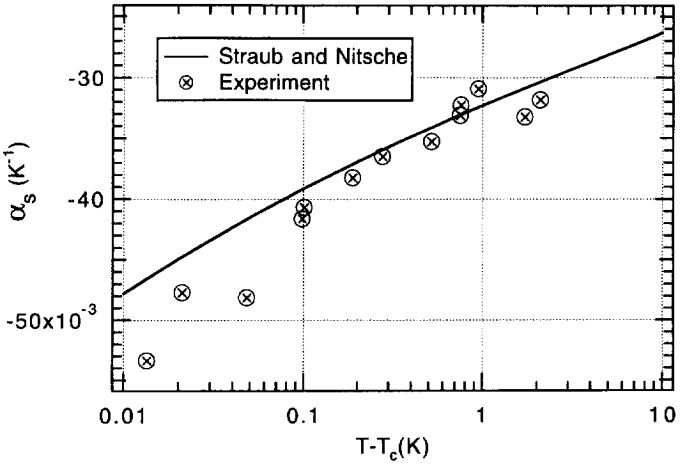

Fig. 4. Comparison of isentropic thermal expansion coefficient α_s between results of this experiment and measurements of Straub and Nitsche [21].

In Fig. 4 the measured values of α_s are compared with the results for α_s calculated from the measured C_V by Straub and Nitsche [21]. It shows a good agreement although, for temperatures closer than 200 mK above T_c, it looks as if our data have the tendency to exceed their curve. The presently obtained accuracy does not permit an accurate fit through our data, therefore, for the calculations in this paper, it seems appropriate to use the values for C_V by Straub and Nitsche [21]. Still, simultaneous measurement of temperature and density changes to produce the isentropic thermal expansion coefficient appears to be a particularly convenient way for probing the theory near T_c.

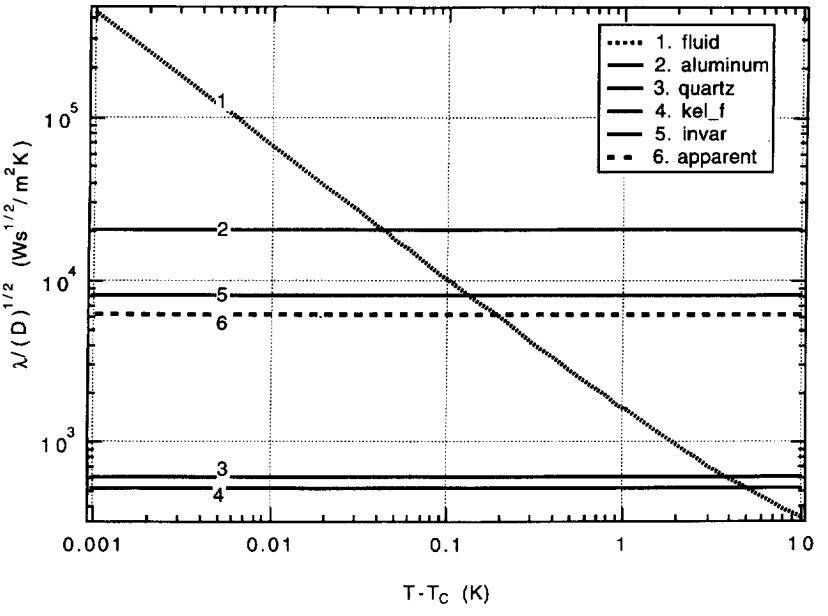

Fig. 5. Comparison between the inverse thermal impedance of the fluid and the wall materials.

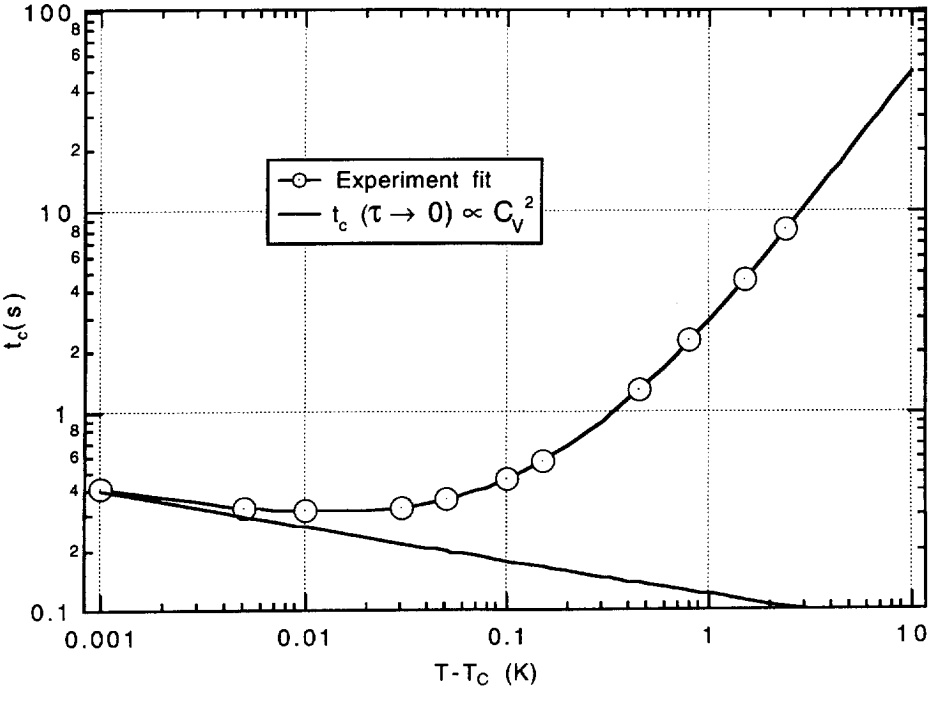

Fig. 6. Variation of the characteristic time scale for isentropic equilibration, t_c, with the distance to T_c.

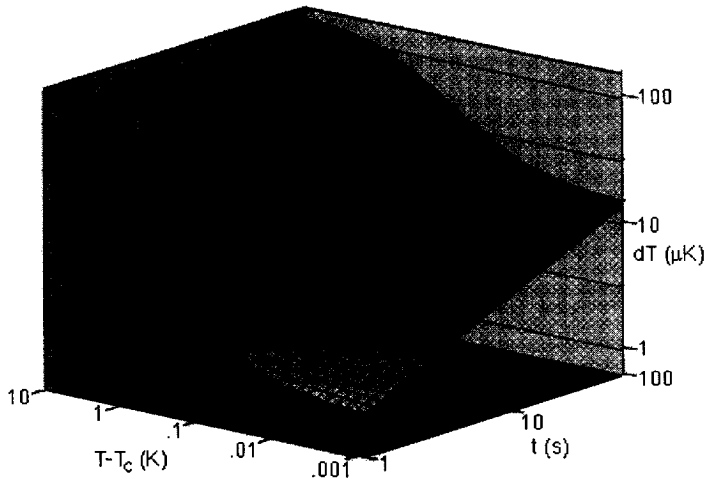

Fig. 7. Theoretical predictions of isentropic temperature rise in our sample fluid accounting for heat losses to the heater substrate and through the other surrounding walls.

Attention is directed next to the comparison between the values of the fluid's inverse thermal impedance [3,15] with the values of the same property of the wall materials. Fig. 5 displays the inverse thermal impedance values against the distance to T_c. It can be clearly seen that for $T - T_c \lesssim 40$ mK the fluid becomes more conductive than any other material of the walls while for $T - T_c \lesssim 200$ mK it even attains a value higher than the apparent inverse thermal impedance. The notion that the finite thermal impedance of the walls governs the energy losses to the surroundings implies then that near $T - T_c = 200$ mK a *conduction crossover* takes place as regards the thermalization time of the sample. This is better demonstrated in Fig. 6 where the characteristic time t_c from Eq. (7), is plotted with respect to distance to T_c. For the calculations presented in Fig. 6 the best-fit values through our data have been employed for the apparent inverse thermal impedance and surface area. It is seen that far away from the critical temperature, t_c appears to decrease rapidly as T_c is approached. Getting closer to T_c it starts gradually to level off and finally a weak rise is observed according to the C_V^2 variation [12], revealing clearly the crossover to a new equilibration regime.

The influence of the finite thermal impedance of the walls to the thermal response of our sample during heating at the boundary, is illustrated in Fig. 7. This is a 3D plot of the predicted isentropic temperature increase [Eq. (10)] versus heating time and distance to the critical point. For clarity, predictions for only one value of dissipated energy (I^2R) are presented. Upon inspection of the graph, it is recognized that, as T_c is approached, there is a characteristic "flattening" of the temperature increase with a square-root time dependence [Eq. (12)]. A little further from T_c, however, the theoretical curves exhibit a prominent peak which becomes higher and broader further in time. This peak originates from the competition between a lower q_f from Eq. (15) and a higher t_c from Eq. (7), as $T - T_c$ increases.

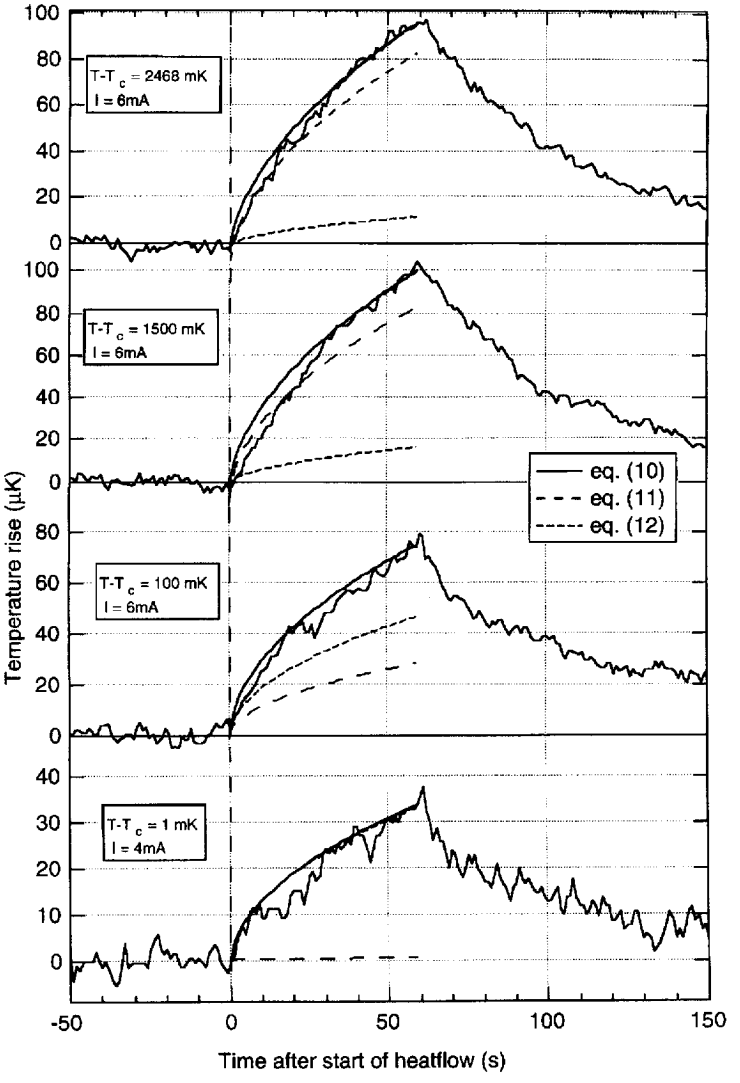

Fig. 8. Thermistor readings during heat pulses (60 s) of constant power at one of the cell walls together with predictions by Eqs. (10)–(12). The heat flow starts at $t = 0$ s.

Typical readings from the thermistor located in the fluid are shown in Fig. 8 during four heating runs each of 60 s duration together with the predictions according to Eqs. (10)–(12). We see that our thermistor responses are essentially synchronous with the onset of heating, an important feature of the AE which is not found when dealing with thermal conduction alone. Comparison with the predictions signifies the validity of Eq. (10). It also demonstrates that for a temperature as close as 1 mK from T_c, the limiting case of Eq. (12) is applicable but that, at $T_c + 2.5$ K, τ is not relatively large enough for the other limiting case [Eq. (11)] to hold. The intermediate

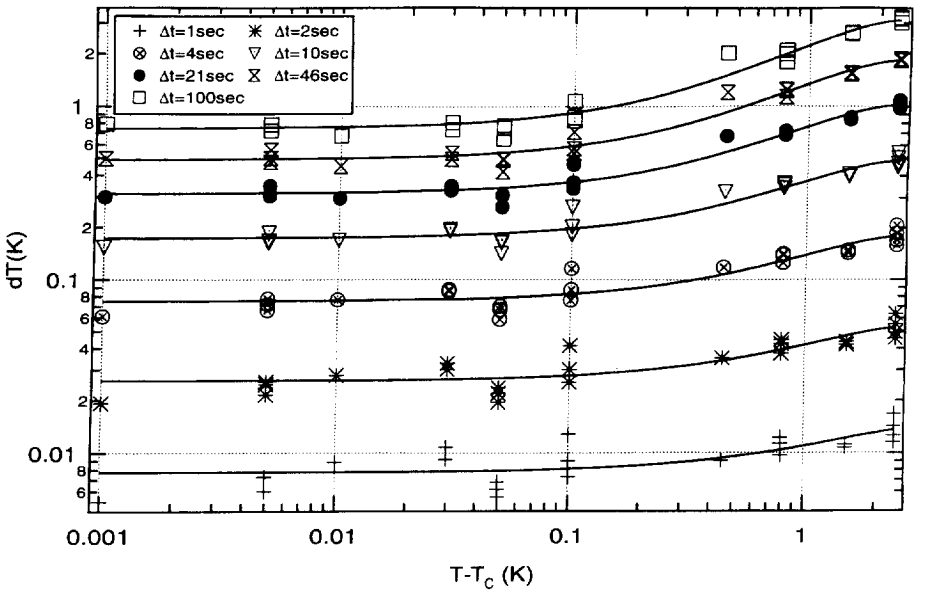

Fig. 9. Experimental data of isentropic temperature rise at several times during heating runs versus the distance to T_c.

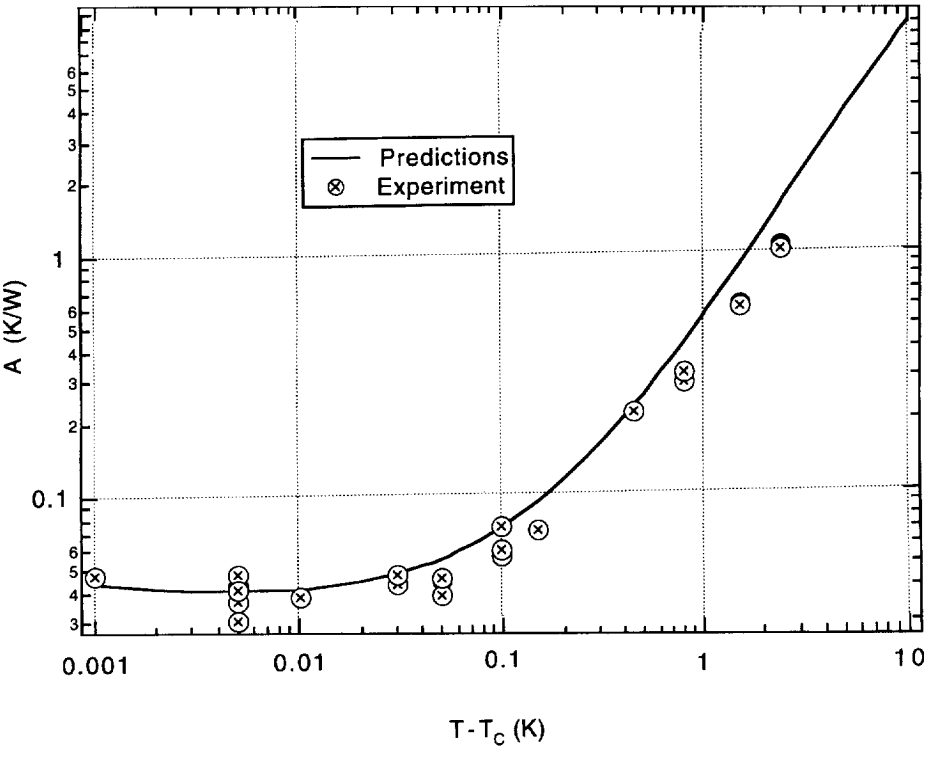

Fig. 10. Comparison between predictions and experiment as regards the amplitude A.

states of $T_c + 1.5$ K and $T_c + 100$ mK do not permit the use of either of the limiting equations.

A complete set of measurements is presented in Fig. 9 where the observed isentropic temperature rise in the bulk is plotted against $T - T_c$ at different times after the onset of heating. The data are normalized with respect to the total dissipated energy (I^2R) entering the fluid [Eq. (15)] in order to facilitate the presentation. Solid lines are best fits through the data. It shows a remarkable similarity between the main features observed experimentally and those outlined theoretically in connection with Fig. 7. Unfortunately, we have not measured far enough from T_c to witness also accurately the behaviour of the peak in the temperature rise.

Fig. 10 shows the measured amplitude A as well as the, according to the apparent properties of the surrounding walls, predicted A versus the distance to the critical point. Again, the experimental data is in good agreement with the predictions manifesting the significance of the role of the properties of the surrounding walls to the thermalization of a critical fluid.

6. Conclusions

The present study provides new theoretical and experimental information regarding the mechanisms of heat transfer in a near-critical fluid. Two dominant mechanisms have been identified: a diffusing thermal boundary layer adjacent to heated surfaces and a homogeneous isentropic temperature change across the entire volume of the sample. This paper is an extension of previous work [11] which dealt with preliminary observations from the same experimental setup. The present study was motivated by the paucity of information in the literature regarding the behaviour of the compression process (AE) in a real experiment of transient heating of a near-critical fluid with bounding walls of finite thermal impedance.

The isentropic temperature rise that follows transient heating of a near-critical fluid has now been determined in a microgravity environment and is described remarkably well by a development of the theoretical model proposed by Ferrell and Hao [12]. The important feature of this description is that the equilibration process is profoundly influenced by the properties of the solid surfaces bounding the fluid even though the isentropic heating effect itself is uniform throughout the bulk of the fluid and is independent of existing gradients. This influence is clearly illustrated by the, now experimentally confirmed, crossover to a new equilibration regime as T_c is approached.

The thermal behaviour of the container can be characterized in the description by means of a single set of phenomenological parameters enabling even in a container of complex geometry the separation of the AE from true heat transport effects in a quantitative way. This conclusion will permit subsequent analysis of the longer-term transient behavior to determine the thermal conductivity and diffusivity of the fluid near to the critical point. Given the difficulty in measuring thermodynamic properties in the near critical region, simultaneous temperature and density measurements,

in microgravity, offer an excellent tool for assessing existing equations of state. The results of the present analysis therefore have a significance beyond the confines of this work.

Acknowledgements

We are indebted to NASA, ESA/ESTEC and the Contractor team headed by DASA-RI for making available the flight opportunity as well as the facility and also for their extensive support in accommodating the experiment. We also want to thank NLR for providing the Remote Operations Site (DUC) in Amsterdam and TPD/TNO at Delft, NL. for the support in designing and manufacturing our Sample Cell Unit. In particular we like to thank Prof. J. Straub, Dr H. vd Berg, B. van Deenen, Dr E. Sakonidou, Dr M. Papadaki and A. Louis for their valuable contribution to the scientific part of this work. A special note of thanks goes to the many colleagues of the workshops of the Van der Waals-Zeeman Institute for their high precision work in the construction of our test cell.

Appendix

To derive the response of the thermistor to changes in the bulk temperature of the fluid, the following situation is considered:

$$T = \begin{cases} T_0 & \text{for } t < -\frac{t_{\text{heat}}}{2}, \\ T_0 + a(t + \frac{t_{\text{heat}}}{2}) & \text{for } -\frac{t_{\text{heat}}}{2} < t < \frac{t_{\text{heat}}}{2}, \\ T_0 + at_{\text{heat}} & \text{for } t > \frac{t_{\text{heat}}}{2}. \end{cases} \tag{A.1}$$

This corresponds to a constant heat input between $t = -t_{\text{heat}}$ and $t = t_{\text{heat}}$ with an isentropic response in the bulk fluid. By taking the Fourier transform, the spectrum density $S(\omega)$ at angular frequency ω is obtained, which is

$$S(\omega) = -\frac{ia}{\pi\omega^2} \sin\left(\omega\frac{t_{\text{heat}}}{2}\right) + \left(a\frac{t_{\text{heat}}}{2}\right)\delta(0), \tag{A.2}$$

where $\delta(x)$ is the Dirac delta function. Fourier analysis is employed here because the solution of the heat flow problem in which the bulk temperature has a simple harmonic variation with time is known, as a standard problem in linear acoustics. Eq. (A.2) shows that the Fourier spectrum is heavily weighted towards low frequencies (much as expected). If we assume now that the thermistor is a homogeneous sphere of radius R then the temperature is:

$$T = T_0 + Aj_0(k_{th}r)\exp(i\omega t) \tag{A.3}$$

where j_0 is the spherical Bessel function of order zero, $k_{th} = \sqrt{-i\omega/D_{th}}$, D_{th} is the thermal diffusivity of the thermistor material, r is the radial coordinate and A is a constant. For $r > R$ it is then

$$T = T_0 + T_1 \exp(i\omega t) + \frac{B}{r} \exp\{i(\omega t - k'r)\}, \tag{A.4}$$

where the first term is the initial temperature, the second is the Fourier component in the bulk, and the third is the thermal boundary layer at the surface of the thermistor (B is a constant). The prime denotes properties of the fluid. Note that the thermal boundary layer takes the form of an outward-going thermal wave which attenuates rapidly with increasing r because of the imaginary part of k'.

The two boundary conditions which determine the constants A and B are those requiring continuity of temperature on and of heat flow through the surface $r = R$. The result is that

$$A_{j_0}(kR) = \frac{T_1}{1+f}, \tag{A.5}$$

where

$$f = -\left(\frac{\lambda}{\lambda'}\right)\left(\frac{kR}{1+ik'R}\right)\frac{j_1(kR)}{j_0(kR)}. \tag{A.6}$$

Notice that, if $f \ll 1$, the surface temperature of the thermistor follows almost exactly the bulk temperature of the fluid at angular frequency ω. Now, as $T \to T_c$, the ratio λ/λ' goes to zero and, since $D' \equiv D_T \to 0$, the term $kR/(1+ik'R)$ also vanishes. Furthermore, as $\omega \to 0$, both the term $kR/(1+ik'R)$ and the ratio of Bessel functions go to zero.

The net result of all this calculation is that, the surface temperature of the thermistor should follow that of the bulk fluid more and more closely as $T \to T_c$.

References

[1] H.E. Stanley, Introduction to Phase Transitions and Critical Phenomena, Clarendon Press, Oxford, 1971.
[2] W.A. Cole, K.M. de Reuck, Int. J. Thermophysics 11 (1990) 189; J.V. Sengers, J.M.H. Levelt Sengers, Ann. Rev. Phys. Chem. 37 (1986) 189; S.N. Biswas, C.A. ten Seldam, Fluid Phase Equilibria 47 (1989) 67.
[3] P. Jany, J. Straub, Int. J. Thermophys. 8(2) (1987) 165.
[4] A. Onuki, H. Hao, R.A. Ferrell, Phys. Rev. A 41 (1990) 2256.
[5] A. Onuki, R.A. Ferrell, Physica A 164 (1990) 245.
[6] H. Boukari, J.N. Shaumeyer, M.E. Briggs, R.W. Gammon, Phys. Rev. A 41 (1990) 2260.
[7] B. Zappoli, D. Baily, Y. Garrabos, B. Le Neindre, P. Guenoun, D. Beysens, Phys. Rev. A 41 (1990) 2264.
[8] H. Boukari, M.E. Briggs, J.N. Shaumeyer, R.W. Gammon, Phys. Rev. Lett. 65 (1990) 2654.
[9] M. Bonetti, F. Perrot, D. Beysens, Y. Garrabos, Phys. Rev. Rap. Com. E 49 (1994) 4779.
[10] J. Straub, L. Eicher, A. Haupt, Phys. Rev. E 51(6) (1995) 5556.
[11] A.C. Michels, R. de Bruijn, T.D. Karapantsios, R.J.J. van Diest, H.R. van den Berg, E.P. Sakonidou, W.A. Wakeham, J.P.M. Trusler, A. Louis, M. Papadaki, J. Straub, Proc. 30th National Heat Transfer Conf., vol. 3, Portland, Oregon, 1995.
[12] R.A. Ferrell, H. Hao, Physica A 197 (1993) 23.

[13] D. Beysens, M. Bonetti, T. Fröhlich, Y. Garrabos, P. Guenoun, B. Le Neindre, F. Perrot, in: M. Costa, R. Rodriquez and A.L. Benavides (Eds.), Lectures on Thermodynamics and Statistical Mechanics, World Scientific, Singapore, 1994, p. 88.
[14] H. Becker, U. Grigull, Wärme-und Stoffübertragung 11 (1978) 9.
[15] A. Abacci, J.V. Sengers, Institute for Physical Science and Technology, Univ. of Maryland, MD, 1990, Technical Report, unpublished.
[16] M. Cork, T. Dewandre, D. Hüser, ESA Bull. 74 (1993) 36.
[17] R.B. Bird, W.E. Stewart, E.N. Lighfoot, Transport Phenomena, Wiley, New York, 1960.
[18] R.H. Huijser, A.C. Michels, N.J. Trappeniers, 1982, Proc. 4th Eur. Symp. on Materials Sciences under Microgravity, Madrid, Spain, 1983 (ESA SP-191), unpublished.
[19] R. de Bruijn, Doctoral Dissertation, Dept. of Physics, Van der Waals-Zeeman Inst., University of Amsterdam, in preparation.
[20] P. Guenoun, B. Khalil, D. Beysens, Y. Garrabos, F. Kammoun, B. Le Neindre, B. Zappoli, Phys. Rev. E 47 (1993) 1531.
[21] J. Straub, K. Nitsche, Fluid Phase Equilibria 88 (1993) 183.